Partial trapping of secondary-electron emission in a Hall thruster plasma

E. Ahedo and F. I. Parra
E.T.S.I. Aeronáuticos, Universidad Politécnica de Madrid, 28040 Madrid, Spain

(Received 18 February 2005; accepted 9 May 2005; published online 23 June 2005)

Secondary-electron emission at the ceramic walls of a Hall thruster modifies the potential jump of the wall Debye sheaths and thus the electron energy losses to the wall. Because of the low plasma collisionality the two counterstreaming beams of secondary electrons are not expected to be totally trapped within the bulk of the discharge. In order to analyze the effects of partial trapping of secondary electrons on the presheath/sheath radial structure, a macroscopic model is formulated. The plasma response depends on the secondary electron emission yield and the trapped fraction of secondary electrons. The sheath potential and wall energy losses are determined mainly by the net current of secondary electrons in the sheaths. For any practical value of the secondary emission yield, the zero-trapping solution is very similar to the zero secondary emission case. Space charge saturation of the sheaths is unattainable for weak trapping. In all cases, secondary electrons have a weak effect on the presheath solution and the ion flux recombined at the walls. © *2005 American Institute of Physics*. [DOI: 10.1063/1.1943327]

I. INTRODUCTION

The performance and lifetime of a Hall thruster (of the long-chamber type) are very much affected by the interaction of the plasma discharge with the dielectric walls. This interaction leads to plasma recombination, electron energy losses, wall collisionality, and ion sputtering.[1–3] At present, an accurate evaluation of these phenomena is not available because of the incomplete understanding and modeling of these processes. The plasma-wall interaction depends mainly on the electron distribution function, which is difficult to know because of the presence of several electron populations, the low collisionality of the plasma, and the contribution of different plasma instabilities. The main or primary electron population is confined by the plasma potential between the two lateral walls, except for a high-energy tail of the distribution collected by the walls. The level of replenishment of this tail by thermalizing collisions is uncertain.[4,5] In addition, the impact of the electron with the ceramic walls can produce a large secondary-electron emission (SEE). Accelerated by the sheaths potentials, secondary electrons enter into the bulk of the plasma as two counterstreaming radial beams. As the SEE increases, the sheath potential decreases and the energy losses into the wall increase.[6] The SEE is also responsible for the near-wall-conductivity and wall collisionality phenomena.[7]

The evolution of the two secondary-electron beams within the thruster chamber depends on the collisional processes acting upon them and the radial structure of the electric potential. Since the transit time between the two chamber walls is very small ($\sim 10^{-8}$ s), it is unlikely that collisional effects trap completely the SEE within the main plasma. For Hall thruster geometries, Jolivet and Roussel[8] were the first to discuss the diffusion/thermalization of the SEE and the possibility of recollection of part of it by the walls. Using a particle-in-cell, presheath/sheath, planar model, they determined the electron distribution function for different cases and showed that partial trapping of the SEE was possible. In this paper we present an alternative, macroscopic model of the general, partial-trapping case. The model is a natural extension of the total-trapping, presheath/sheath model of Ahedo.[9] The goal is to obtain general, semianalytical results on the potential structure and energy losses in terms of both the SEE yield and the trapped fraction of the SEE beams. The zero-trapping limit is discussed too.

The rest of this paper is organized as follows. In Sec. II we present the fundamentals of the model. In Secs. III and IV we solve the sheath and presheath problems, respectively. Conclusions are presented in Sec. V.

II. THE PLANAR PARTIAL-TRAPPING MODEL

A sketch of geometrical and physical aspects of the model is shown in Fig. 1. In order to focus the study on partial-trapping effects, we consider the thruster chamber to be planar, with lateral walls made of identical materials. Thus symmetry considerations with respect to the chamber midplane are applicable. The analysis will be centered on the half-chamber MW, between the central surface M and the external wall W.

A macroscopic formulation with one ion species (i) and several electron populations is proposed. The basic hypotheses of the presheath/sheath model of Ref. 9 are the following. First, the plasma Debye length λ_d is much smaller than any other relevant length of the problem. Second, walls are dielectric, secondary electrons are produced by bombardment of primary electrons, and their emission energy is of the order of the wall temperature T_w. And third, the magnetic field is assumed radial and all magnetic effects (such as the $E\times B$ drift of the secondary and primary populations, and magnetic mirroring) are ignored. These assumptions justify an unmagnetized, sheath/presheath/sheath formulation and a radial potential profile $\phi(r)$ with a single maximum at the center of the channel. Let Q and Q' be the transition points between the presheath and the two Debye sheaths (Fig. 1).

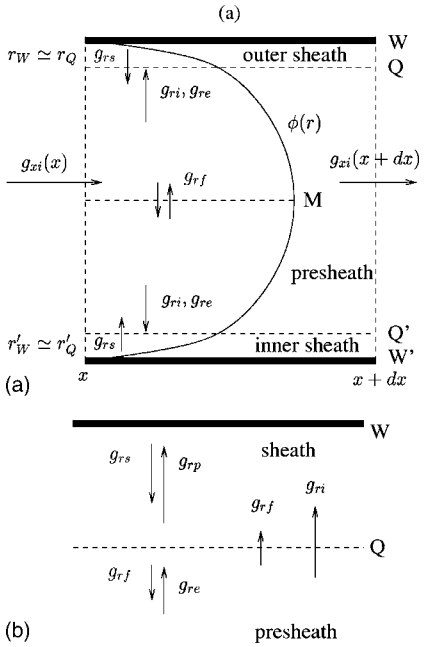

FIG. 1. Sketch of the planar partial-trapping model in (a) presheath and (b) sheath at a given axial position.

Typically, the wall temperature is much smaller than the sheath potential drop ϕ_{WQ}. Therefore, after crossing the sheath WQ, secondary electrons emitted at wall W practically form a monoenergetic beam at point Q. The electric potential of the presheath still accelerates radially that beam towards the channel center M. Then, the beam is decelerated in the other half channel, region MQ' and sheath $Q'W'$. If that radial crossing of the secondary electrons is collisionless, they will reach the opposite wall W' with the same (small) radial velocity they had when emitted at W and will be collected by wall W' (the reflection of electrons at the walls is either neglected or included as a part of the SEE yield). However, collisions with other particles or wave interaction would reduce the radial energy of the SEE beam between points Q and Q', and could prevent it (or part of it) from reaching the wall W'. In this case, secondary electrons remain trapped within the chamber and thermalize eventually with the main population of confined electrons. The same considerations apply to the SEE beam emitted from the wall W'.

Reference 9 considered the total-trapping case when the whole SEE beams thermalize with the primary electron population. The main difficulty on modeling this problem was how to treat the SEE as a monoenergetic beam near the emission wall and as a confined population in the bulk of the plasma. Different distributions for the electron populations in sheaths and presheath were used, and a consistent matching at the sheath/presheath transitions was carried out. Here, in order to deal with the general, partial-trapping case, we make a further division of the electron populations. Each SEE beam is split into (i) a *trapped* (sub)beam which thermalizes with the main confined population and (ii) a *free* (sub)beam which is collected back at the opposite wall. A trapping fraction δ_t is defined to divide each SEE beam flux into the two sub-beams. Reference 9 treated the case $\delta_t=1$. In the opposite, zero-trapping limit, $\delta_t=0$, the two SEE beams (which are identical except for the velocity direction) cross freely the region between the two walls and are collected back at the opposite wall, leaving no net particle contribution to the discharge.

For the general case, the electron populations defined in each region are illustrated in Fig. 1: (a) In the sheath QW there are the population p of primary, confined electrons, the population s of secondary electrons emitted by the adjacent wall W, and the population f of free, secondary electrons emitted by the opposite wall W' and collected by wall W. (b) In the presheath $Q'Q$ there are the population e of confined electrons (which includes population p plus the trapped fraction of the SEE populations emitted by the two walls) and the two counterstreaming populations f of free, secondary electrons.

The study here is devoted to evaluate the effect of different degrees of SEE trapping on the radial structure. The determination of the correct value of δ_t in terms of the different collisional processes is out of the scope of this work, but some basic considerations, justifying the interest of weak SEE trapping, are made in the Appendix.

III. THE SHEATH SOLUTION

The model of the collisionless sheath QW consists of the quasiplanar Poisson equation plus the conservation equations for the ions i and the three electron species (p, s, and f). Following Refs. 6,9, these are

$$n_\alpha v_{r\alpha} \equiv g_{r\alpha} = \text{const} \quad (\alpha = i,s,f,p), \tag{1}$$

$$n_p = n_{pQ} \exp \frac{e(\phi - \phi_Q)}{T_p}, \tag{2}$$

$$g_{rpW} = n_{pQ} \exp \frac{-e\phi_{WQ}}{T_p} \sqrt{\frac{T_p}{2\pi m_e}}, \tag{3}$$

$$\tfrac{1}{2} m_i v_{ri}^2 + \tfrac{5}{2} T_i + e\phi = \text{const}, \tag{4}$$

$$T_i n_i^{-2/3} = \text{const}, \tag{5}$$

$$n_f = (1-\delta_t) n_s, \tag{6}$$

$$v_{rf} = -v_{rs} \simeq \left[\frac{2e(\phi - \phi_W)}{m_e} \right]^{1/2}. \tag{7}$$

Here symmetry properties have been applied to define v_{rf}; the kinetic energy of the SEE at the emission point has been neglected (i.e., $T_w/T_p \to 0$); the plasma density at Q, n_{iQ}, and the ion flux, g_{riQ}, are given by the presheath solution; and Eq. (3) for the flux of primary electrons is based on a quasi-Maxwellian distribution at the presheath transition. [A depletion factor should be added on the right-hand side of Eq. (3) if the collected tail of the distribution is not replenished totally; this effect, although very interesting, is not the subject of this work. Also, a correction term should be included in Eq. (2) to take into account that electrons are not reflected

back by the wall, but its effect on the sheath solution is small.]

The flux of secondary electrons from the wall W is

$$g_{rsW} = -\delta_w g_{rpW}, \tag{8}$$

where δ_w is the effective SEE yield, which depends on T_p and the wall material.[10,11] The flux of secondary electrons emitted at the wall W' and reaching the sheath QW is

$$g_{rfQ} = -(1-\delta_t) g_{rsW}. \tag{9}$$

Finally, the zero-current condition establishes that

$$g_{riQ} = g_{rpW} + g_{rsW} + g_{rfQ} \tag{10}$$

or, using above equations,

$$g_{riQ} = (1-\delta_w\delta_t) g_{rpW}, \tag{11}$$

where $\delta_w\delta_t g_{rpW}$ is the *net secondary* electron flux.

The sheath equations are solved as in Ref. 9. Here, the main steps are mentioned briefly. Parameters T_p and n_{iQ} are used to nondimensionalize the sheath equations and hats are used to distinguish most of the nondimensional variables (i.e., $\hat{\phi}=e\phi/T_p$). The natural spatial variable in the sheath is

$$\zeta = (r-r_W)/\lambda_d, \tag{12}$$

with $\lambda_d=\sqrt{\epsilon_0 T_p/e^2 n_{iQ}}$.

Applying the boundary condition $d(e\phi/T_p)/d\zeta|_Q=0$, the integration of the quasiplanar Poisson equation yields

$$\frac{e^2 n_{iQ}}{2T_p}\left(\frac{d\phi}{d\zeta}\right)^2 = U(e\phi) - U(e\phi_Q), \tag{13}$$

with

$$U(e\phi) = n_p T_p + (n_s+n_f) m_e v_{rs}^2 + (m_i v_{ri}^2 + T_i) n_i \tag{14}$$

being the Sagdeev's potential. The two other boundary conditions at point Q are plasma quasineutrality,

$$0 = U'_Q \equiv n_{pQ} + n_{sQ} + n_{fQ} - n_{iQ}, \tag{15}$$

and the Bohm condition,

$$0 = U''_Q \equiv \left(\frac{n_p}{T_p} - \frac{n_s+n_f}{m_e v_{rs}^2} - \frac{n_i}{m_i v_{ri}^2 - \frac{5}{3}T_i}\right)_Q. \tag{16}$$

Solving this last one for the ion velocity, one has

$$m_i v_{riQ}^2 = \frac{2e\phi_{WQ} T_p n_{iQ}}{2e\phi_{WQ} n_{pQ} - T_p(n_{sQ}+n_{fQ})} + \frac{5}{3}T_{iQ}, \tag{17}$$

which is the generalized sonic condition for the incoming ion flow. It will be found that $n_{sQ}+n_{fQ} \ll n_{pQ}$, so that $v_{riQ} \simeq \sqrt{(T_p+5T_{iQ}/3)/m_i}$.

The dimensionless sheath solution depends on three parameters: δ_w, δ_t, and $\hat{T}_{iQ} \equiv T_{iQ}/T_p$. The last parameter is generally small and its influence has already been studied in Ref. 9. Here it is included for completeness but results are presented for $\hat{T}_{iQ}=0$ only. Using Eqs. (3) and (11) the sheath potential drop is

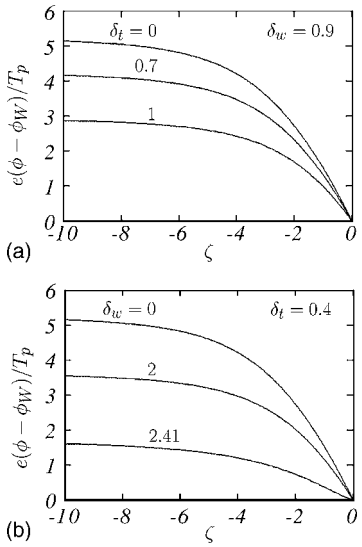

FIG. 2. Sheath solution. Profiles of the electrostatic potential for (a) $\delta_w=0.9$ and several values of δ_t from 0 to 1; (b) $\delta_t=0.4$ and several values of δ_w from 0 up to the charge-saturation limit.

$$\hat{\phi}_{WQ} = \ln\sqrt{\frac{m_i}{2\pi m_e}} + \ln(1-\delta_t\delta_w) + \ln\left(\frac{n_{pQ}}{n_{iQ}}\sqrt{\frac{T_p}{m_i v_{riQ}^2}}\right). \tag{18}$$

Figures 2(a) and 2(b) show potential profiles for different values of δ_t and δ_w. Figures 3(a) and 3(b) show the profiles of the different plasma densities for (a) the zero-emission case and (b) 200% of SEE and zero trapping. Notice that even for such high secondary-electron emission, the density of secondary electrons is very small except in the very vicinity of the wall. This justifies that $\hat{\phi}$, $\hat{n}_i$, and $\hat{n}_p$ depend on δ_t and δ_w only through their product $\delta_t\delta_w$. In other words, the sheath solution depends mainly on the net

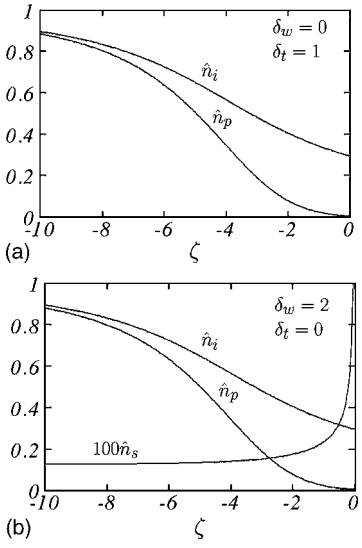

FIG. 3. Sheath solution. Profiles of the densities of the different species for (a) $\delta_w=0$, and (b) $\delta_w=2$ and $\delta_t=0$. In this and next figures $\hat{T}_{iQ}=0$. Notice that $n_f=n_s$ and the curves are plotted 100 times these densities. In the sheath scale the presheath is at $\zeta_Q=-\infty$.

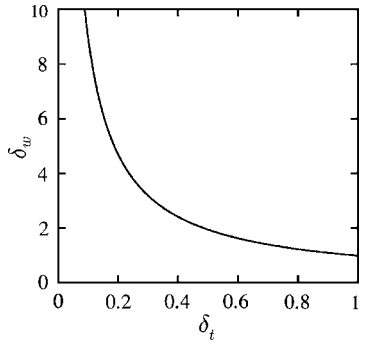

FIG. 4. SEE yield vs the trapped fraction at the charge-saturation limit.

secondary-electron current. The second conclusion, implicit in Eq. (18) too, is that SEE affects the sheath solution significantly only when $\delta_t\delta_w$ approaches one.

A. The charge-saturation regime

When the product $\delta_t\delta_w$ becomes close to one, the sheath approaches the charge-saturation limit (CSL). This limit is characterized by the condition $d\phi/d\zeta|_W=0$ or, using Eq. (13), by

$$0 = U(e\phi_W) - U(e\phi_Q). \tag{19}$$

This CSL condition can be expressed as a relation of the form $\delta_w=\delta_w^*(\delta_t,\hat{T}_{iQ})$, but the influence of $\hat{T}_{iQ}$ can be disregarded.[9] Figure 4 depicts $\delta_w=\delta_w^*(\delta_t)$. As the trapped fraction δ_t decreases, δ_w^* increases and attains very large values for $\delta_t\ll 1$. One has

$$\begin{aligned} 1-\delta_w^* &\simeq 8.31\sqrt{m_e/m_i} \quad \text{for } \delta_t = 1, \\ \delta_w^* &\simeq 0.24\sqrt{m_i/m_e} \quad \text{for } \delta_t = 0. \end{aligned} \tag{20}$$

If δ_{wm} is the maximum SEE yield of the wall material and $\delta_{wm}\delta_t<1$, the sheath can never reach the charge-saturation limit. In practice, the maximum SEE yield is about 1–2 for metallic materials and 2–5 for certain dielectrics.[8,12,13] Therefore, charge saturation of the sheaths can occur only for high SEE trapping. Moreover, for $\delta_{wm}\delta_t<0.6$, say, the effects of the SEE flux on the sheath solution are marginal.

For wall and plasma conditions leading to $\delta_w>\delta_w^*(\delta_t)$, the sheath is in the charge-saturated regime (CSR). A potential well, $\Delta_w\phi\simeq(T_w/e)\ln(\delta_w/\delta_w^*)$, is formed near the wall to reduce the s flux actually crossing the sheath to $\delta_w^* g_{rpW}$. For $T_w/T_p\to 0$, $\Delta_w\phi/\phi_{WQ}$ is negligible and the dimensionless solution for the charge-saturation regime is the solution for the charge saturation limit.[9]

The CSL relation $\delta_w=\delta_w^*(\delta_t)$ can be explained from the pressure balance implicit in Eq. (19).[9] The dominant terms in Eq. (19) at the CSL satisfy

$$\sqrt{\frac{m_i}{m_e}} \sim \frac{|g_{rs}|+g_{rf}}{g_{ri}} \equiv \frac{(2-\delta_t)\delta_w^*}{1-\delta_t\delta_w^*}. \tag{21}$$

Based on this estimate, the expression

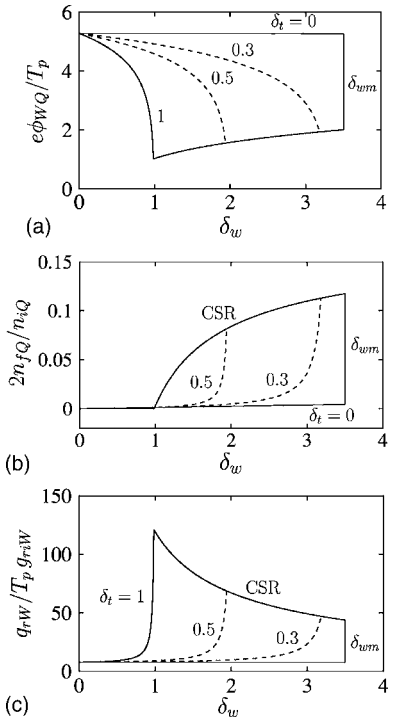

FIG. 5. Parametric region of solutions, in terms of δ_w and δ_t, for (a) the sheath potential drop, (b) the density of free secondary emission at point Q, and (c) the radial losses of energy. The limits are zero-trapping, total-trapping, charge-saturation, and maximum SEE yield (here $\delta_{wm}=3.5$)

$$\frac{1-\delta_t\delta_w^*}{(2-\delta_t)\delta_w^*}\sqrt{\frac{m_i}{m_e}} = 2.35 + 5.64\delta_t \tag{22}$$

is found to fit excellently the exact solution of $\delta_w^*(\delta_t)$; in fact, differences are unobservable in the scale of Fig. 4.

Finally, from Eq. (21) the relative magnitudes of the fluxes of the different species at the CSR follow

$$\begin{aligned} |g_{rs}| &\sim g_{rp} \gg g_{ri} \quad \text{if } \delta_t = O(1), \\ |g_{rs}| &\simeq |g_{rf}| \gg g_{rp} \simeq g_{ri} \quad \text{if } \delta_t \ll 1, \end{aligned} \tag{23}$$

which illustrates that the level of SEE trapping modifies the balance among the different plasma currents at the wall.

B. Influence of the SEE parameters

In the parametric plane (δ_w,δ_t) the region where a sheath solution exists is bounded by four limit cases: (i) total trapping ($\delta_t=1$), (ii) zero trapping ($\delta_t=0$), (iii) sheath charge saturation ($\delta_w=\delta_w^*$), and (iv) maximum SEE yield ($\delta_w=\delta_{wm}$).

Figure 5(a) shows the evolution of $\hat{\phi}_{WQ}$ with δ_w and δ_t. The dimensionless sheath potential ranges from about 5.3 for zero SEE or zero trapping to about 1–2 at the CSR. Figure 5(b) depicts $2n_{fQ}/n_{iQ}$, which is the ratio of the free electron density to the total plasma density at the presheath/sheath transition. This ratio has a maximum of about 10% for the CSR and $\delta_t\ll 1$. Since n_f still decreases slightly within the presheath, we expect the free SEE beams to have a marginal role in the presheath solution.

A relevant magnitude is the heat deposited at the walls by ions and electrons impacting them. The energy flux (per unit of lateral area) is

$$q_{rW} = 2T_p g_{rpW} + \left(\tfrac{1}{2} m_i v_{riW}^2 + \tfrac{5}{2} T_{iW}\right) g_{riW} \tag{24}$$

[the radial flux of axial energy, $1/2 m_i v_{riW}^2 g_{riW}$, which is (partially) external to the model is not included in q_{rW}]. Using the different sheath relations, the (dimensionless) energy flux deposited at the wall follows

$$\hat{q}_{rW} \equiv \frac{q_{rW}}{T_p g_{riQ}} = \frac{2}{1-\delta_w \delta_t} + \hat{\phi}_{WQ} + \frac{1}{2} + \frac{(1+2\hat{\phi}_{WQ})(2-\delta_t)\hat{n}_{sQ}}{2[2\hat{\phi}_{WQ} - (1+2\hat{\phi}_{WQ})(2-\delta_t)\hat{n}_{sQ}]} + \frac{10}{3}\hat{T}_{iQ}, \tag{25}$$

where the two last terms are small. Since both T_p and g_{riQ} depend mainly on the presheath solution, the dimensionless energy flux $\hat{q}_{rW}$ is the magnitude actually determined by the sheath. Figure 5(c) shows that $\hat{q}_{rW}$ ranges from about 8 for $\delta_w \delta_t \ll 1$ to about 100 at the CSR.

IV. THE PLANAR PRESHEATH SOLUTION

The plasma in the presheath consists of the ion population (i), the two symmetric counterstreaming populations of free electrons (f), and a population of confined electrons (e). This last one includes population p plus the trapped fraction of secondary electrons emitted from the two walls. Thus, at the presheath/sheath transition point Q, one has

$$n_{eQ} = n_{pQ} + \delta_t n_{sQ}, \qquad g_{eQ} = g_{pQ} + \delta_t g_{sQ}. \tag{26}$$

The relation between T_e and T_p is determined below by equating the Bohm conditions at the two sides of point Q.

According to the presheath analysis of Ref. 14, the pertinent equations for a planar chamber consist of Eqs. (1) and (7) for each of the two free populations f, and

$$\frac{\partial}{\partial r} g_{ri} = \nu_w n_i, \tag{27}$$

$$m_i g_{ri} \frac{\partial v_{ri}}{\partial r} = -\frac{\partial}{\partial r}(n_i T_i) - e n_i \frac{\partial \phi}{\partial r} - \nu_r m_i g_{ri}, \tag{28}$$

$$\frac{\partial}{\partial r}\left(\frac{3}{2} T_i g_{ri}\right) + T_i n_i \frac{\partial}{\partial r}(v_{ri}) = \nu_i \frac{1}{2} m_i v_{ri}^2 n_i + \frac{5}{2} \nu_w n_i T_i, \tag{29}$$

$$n_e = n_{eQ} \exp \frac{e(\phi - \phi_Q)}{T_e}, \tag{30}$$

$$n_i = n_e + 2n_f, \tag{31}$$

$$g_{re} = g_{ri}, \tag{32}$$

with ν_i the ionization frequency, ν_w the net plasma production frequency, and ν_r an effective friction frequency.[14] The two last parameters include effects of both the gas ionization (i.e., ν_i) and axial variations of the axial flow.

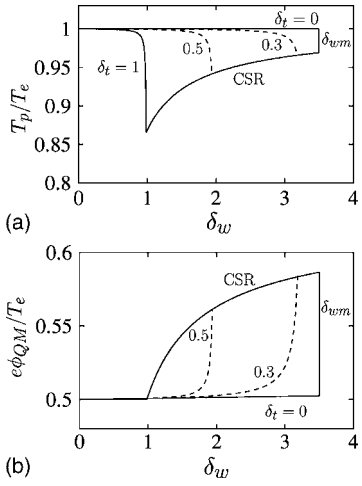

FIG. 6. (a) Temperature ratio of confined electron populations and (b) presheath potential drop in terms of δ_w and δ_t. Other parameters are $\tilde{\nu}_r$, $\tilde{\nu}_i$, $\tilde{T}_{iM}=0$, and $\delta_{wm}=3.5$.

Solving the presheath equations for the derivatives of the plasma variables, one finds that they become singular at the point where

$$0 = \frac{n_e}{T_e} - \frac{2n_f}{m_e v_{rf}^2} - \frac{n_i}{m_i v_{ri}^2 - \frac{5}{3} T_i}. \tag{33}$$

In particular, the electric field becomes infinite there, indicating that the singularity corresponds to the transition point Q to the sheath, where a much shorter scale dominates. Solving Eq. (33) for the ion velocity yields the Bohm condition at the presheath side of point Q,

$$m_i v_{riQ}^2 = \frac{e\phi_{WQ} T_e n_{iQ}}{e\phi_{WQ} n_{eQ} - T_e n_{fQ}} + \frac{5}{3} T_{iQ}. \tag{34}$$

Both Eqs. (17) and (34) are generalized forms of the Bohm sonic condition for multispecies plasmas.[9] Physically, the sonic condition on a single fluid is related to the balance between dynamic and static pressures. In the present multispecies plasma, the *quasineutral* electrostatic interaction of the ions with several electron populations is felt like an extra pressure term by the ion fluid.

For v_{riQ} to satisfy both Eqs. (17) and (34), it must be

$$\frac{n_{eQ}}{T_e} = \frac{n_{pQ}}{T_p} - \frac{\delta_t n_{sQ}}{2e\phi_{WQ}}, \tag{35}$$

which relates T_e and T_p and completes the matching of the presheath and sheath problems. Figure 6(a) plots the ratio T_p/T_e which is between 0.86 and 1 for the whole parametric range of sheath solutions. Notice that $T_e=T_p$ for $\delta_w=0$ or $\delta_t=0$, as expected. (The difference between the temperatures of species p and e has been ignored in other models.[15,16])

Using T_e (instead of T_p), n_{iQ}, and ν_w to nondimensionalize the presheath equations, one finds that these depend on dimensionless parameters δ_w, δ_t, T_{iQ}/T_e, ν_i/ν_w, and ν_r/ν_w. Since the sheath solution is known from the preceding section, it is convenient to integrate the presheath problem from point Q towards point M. The integration ends when $v_{ri}=0$

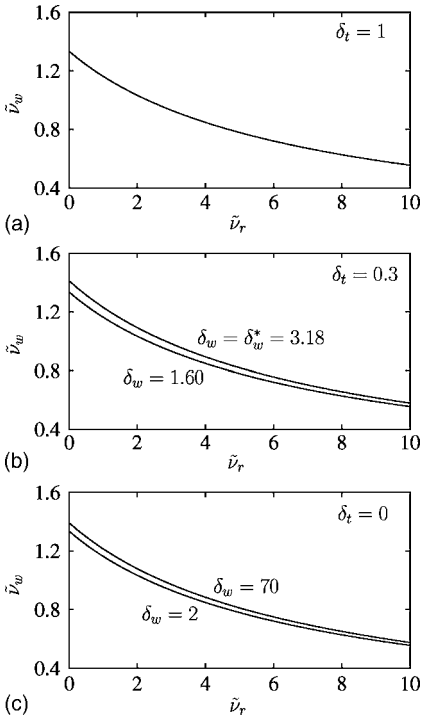

FIG. 7. The net production frequency vs the radial friction frequency for different values of δ_t and δ_w; other parameters are $\tilde{\nu}_i, \tilde{T}_{iM}=0$.

and [since $h_c \simeq 2(r_Q - r_M)$ in the presheath scale] determines $h_c \nu_w (T_e/m_i)^{-1/2}$ as a function of the above five parameters. Calling

$$\tilde{\nu}_j = \nu_j \times h_c (T_e/m_i)^{-1/2}, \quad j = w,r,i, \tag{36}$$

and solving the resulting parametric function for $\tilde{\nu}_w$, one ends with

$$\tilde{\nu}_w = \tilde{\nu}_w(\delta_w, \delta_t, \tilde{\nu}_i, \tilde{\nu}_r, T_{iQ}/T_e). \tag{37}$$

This is the *plasma balance equation* which determines the *net* volumetric plasma production required to compensate the plasma recombined at the walls.[17] Therefore, at a given radial section, the plasma contribution from the axial flow is $\partial(n_e v_{xi})/\partial x \sim n_i(\nu_w - \nu_i)$.

Figures 7(a)–7(c) depict the production frequency in terms of the two parameters characterizing the SEE response, δ_w and δ_t. The effect of the SEE is small because of $T_p/T_e \sim 1$ and $2n_f/n_i \ll 1$ [Fig. 5(b)]. With respect to the influence of $\tilde{\nu}_r$, $\tilde{\nu}_i$, and T_{iQ}/T_e, Ref. 14 showed that $\tilde{\nu}_w$ depends almost exclusively on the first one. The implicit form of the function $\tilde{\nu}_w(\tilde{\nu}_r)$ (exact for $T_{iQ}/T_e=0$, $\tilde{\nu}_i=0$, and $\delta_t=1$) is[14]

$$\frac{\tilde{\nu}_w + \tilde{\nu}_r}{\sqrt{\tilde{\nu}_w \tilde{\nu}_r}} \arctan \sqrt{\frac{\tilde{\nu}_r}{\tilde{\nu}_w}} - 1 = \frac{\tilde{\nu}_r}{2}, \tag{38}$$

which is plotted in Fig. 7(a).

Figure 6(b) shows that the effect of partial trapping on the presheath potential drop, $\phi_{QM} = \phi_M - \phi_Q$, is less than 20%. The curves represent the expression

$$\frac{e\phi_{QM}}{T_e} = \frac{1}{2} \times \left(\frac{n_{eQ}}{n_{iQ}} - \frac{T_e}{e\phi_{WQ}} \frac{n_{fQ}}{n_{iQ}} \right)^{-1} \sim \frac{1}{2} \tag{39}$$

obtained from Eqs. (28) and (34) for $T_{iM}, \nu_i, \nu_r = 0$.

V. CONCLUSIONS

The degree of trapping of the SEE beams within the bulk of the plasma is found to have an important effect on the potential drop and the charge-saturation limit of the sheath. The structure of the sheaths depends mainly on the *net* SEE current crossing it, that is, the difference between the currents of the beam emitted at the wall next to the sheath and the free fraction of the beam emitted by the opposite wall. More precisely, the sheath solution depends on the parameter $\delta_t \delta_w$ representing the relative net secondary current. Therefore, the main results of Ref. 9 for $\delta_t = 1$ are extendible to the general trapping case by just substituting δ_w by $\delta_t \delta_w$. To this respect, we stand out that electron energy losses to the walls depend on $\delta_t \delta_w$, differences with the classical sheath solution for zero SEE are significant only when $\delta_t \delta_w$ approaches one, the charge-saturation limit is reached for $\delta_t \delta_w \simeq 98.3\%$ (for xenon), and the case of zero trapping of SEE behaves like the zero SEE case.

The differences between the zero SEE case ($\delta_w = 0$) and cases with high SEE and low trapping (i.e., $\delta_w \gg 1$ and $\delta_t \ll 1$) lie only on a large density of secondary electrons *in the very vicinity* of the walls. This SEE density decreases rapidly across the sheaths and is always small in the presheath. As a consequence, the effect of the two free secondary beams on the presheath is negligible and the presheath solution for total trapping is a good approximation for all the SEE cases. This means that the plasma balance equation, which determines the ion current that recombines at the walls, is affected weakly by SEE.

The importance of the trapping level of the SEE on both the electron energy losses and the impact energy of ions at the walls recommends to investigate more deeply the phenomena affecting the trapping of secondary electrons (including plasma-wave interactions) and to develop models capable of determining accurate values of δ_t along the thruster chamber. Also, particle-simulation codes capable of following separately the populations of primary and wall-emitted electrons could be very helpful to advance in this problem.

This work has treated only the case of a planar channel. For a Hall-thruster cylindrical channel, there is some asymmetry between the solutions at the inner and outer radial parts of the channel,[9,14] but the fundamental conclusions of the present study continue to be valid. Thus, the influence of SEE on the cylindrical presheath is going to be small for any trapping degree, and a fraction of free secondary electrons will slow down the reduction of the sheath potential caused by the SEE. But, at the same time, a new situation, not studied here, can arise when the presheath asymmetry leads to different potentials at the two presheath boundaries, more particularly, when $e|\phi_Q - \phi_{Q'}| \gg T_w$. For total trapping, the two sheaths behave identically and thus the two wall potentials are different, $e|\phi_W - \phi_{W'}| \gg T_w$.[9] But, for low or zero trapping, we expect a solution with (i) a different recollection

of the free SEE beams at each wall and (ii) almost identical wall potentials, i.e., $e|\phi_W - \phi_{W'}| \leqslant O(T_w)$. The main consequence of this response would be different energy fluxes at each lateral wall.

ACKNOWLEDGMENTS

This work was sponsored by the Air Force Office of Scientific Research, Air Force Material Command, USAF, under Grant No. FA8655-04-1-3003, and by the Ministerio de Educación y Ciencia of Spain (Project No. ESP2004-03093).

APPENDIX: SOME CONSIDERATIONS ON THE BEAM TRAPPING

The first point is that trapping of the secondary monoenergetic beams could be different for short-range (strong) collisions, such as those with neutrals, than for collective (weak) collisions, such as those of an electron with a cloud of ions or those representing electron-wave interaction.

For short-range, electron-neutral (e-n) collisions, it is plausible to assume that a fraction of the beam suffers strong collisions, which eliminate totally the directed radial energy, whereas the rest of the beam crosses the presheath unaffected. If λ_{en} is the electron-neutral mean-free path, the trapped fraction of the beam is

$$\delta_t = 1 - \exp(-h_c/\lambda_{en}). \tag{A1}$$

For the 1 kW class Hall thruster, typical values are $h_c \sim 15$ mm and $n_n \sim 10^{19}$ m^3, yielding $\lambda_{en} \sim 30$ cm and $\delta_t \sim h_c/\lambda_{en} \sim 5\%$. Therefore, the SEE beams are weakly trapped by electron-neutral collisions.

Let us consider now the long-range, weak, momentum-transfer collisions between a monoenergetic SEE beam and clouds of ions and primary electrons. For this case, it seems more correct to consider that the whole SEE beam loses the radial momentum progressively. The beam will be totally trapped or untrapped depending on the amount of directed radial energy it loses. One can measure this loss from

$$\frac{d}{dr}\left(\frac{1}{2}m_e v_{rs}^2 - e\phi\right) = -m_e \nu_c v_{rs}, \tag{A2}$$

where[18]

$$\nu_c = \frac{(n_e + n_i)e^4 \ln \Lambda}{4\pi\epsilon_0^2 m_e^2 v_{rs}^3} \tag{A3}$$

includes the effects of both ions and (confined) electrons on the SEE beam. Since the potential drop in the presheath is weak and in order to integrate Eq. (A2) between Q' and Q, we can take $m_e v_{rs}^2/2 \simeq e\phi_{WQ}$. Then, for the beam emitted at W', one has

$$\tfrac{1}{2}m_e v_{rsW}^2 = \tfrac{1}{2}m_e v_{rsW'}^2 + e\phi_{W'W} - \Delta_c\left(\tfrac{1}{2}m_e v_{rs}^2\right), \tag{A4}$$

with

$$\Delta_c\left(\frac{1}{2}m_e v_{rs}^2\right) \simeq \frac{h_c n_e e^3 \ln \Lambda}{4\pi\epsilon_0^2 \phi_{W'Q'}}, \tag{A5}$$

and $\phi_{W'W} = \phi_W - \phi_{W'}$ (=0 for the planar case). Thus the beam will be trapped when $m_e v_{rsW}^2 < 0$. For $2n_e = 10^{18}$ m^{-3}, $\ln \Lambda = 14$, and $\phi_{W'Q'} = 50$ V, one has $\Delta_c(m_e v_{rs}^2/2) \sim 0.055$ eV $\equiv 650$ K, which is very small compared with the beam energy on the presheath, but of the order of the energy of secondary electrons when they were emitted.

These simple considerations show that total, weak, and zero trapping of SEE are possible. Furthermore different situations are likely along the thruster chamber because of the different plasma conditions. The uncertainty on the level of trapping indicates that a more rigorous study, based on distribution functions and including beam thermalization due to electron-electron and electron-wave interactions, is needed.

[1] V. Zhurin, H. Kaufman, and R. Robinson, Plasma Sources Sci. Technol. **8**, R1 (1999).
[2] A. Morozov and V. Savelyev, *Reviews of Plasma Physics* (Kluwer Academic, New York, 2000), Vol. 21, Chap. 2.
[3] E. Ahedo, J. Gallardo, and M. Martínez-Sánchez, Phys. Plasmas **10**, 3397 (2003).
[4] N. Meezan and M. Capelli, *Proceedings of the 27th International Electric Propulsion Conference, Pasadena, CA, USA* (Electric Rocket Propulsion Society, Cleveland, Ohio, 2001), IEPC-01-051.
[5] O. Batishev and M. Martínez-Sánchez, *Proceedings of the 28th International Electric Propulsion Conference, Toulouse, France* (Electric Rocket Propulsion Society, Cleveland, OH, 2003), IEPC-03-188.
[6] G. Hobbs and J. Wesson, Plasma Phys. **9**, 85 (1967).
[7] A. Morozov, Y. Esipchuk, G. Tilinin, A. Trofimov, Y. Sharov, and G. Y. Shchepkin, Sov. Phys. Tech. Phys. **17**, 38 (1972).
[8] L. Jolivet and J.-F. Roussel, *SP-465: 3rd Spacecraft Propulsion Conference, Cannes, France* (European Space Agency, Noordwijk, The Netherlands, 2000), p. 367.
[9] E. Ahedo, Phys. Plasmas **9**, 4340 (2002).
[10] J. Fife, M. Martínez-Sánchez, and J. Szabo, *Proceedings of the 33rd Joint Propulsion Conference, Seattle, WA* (American Institute of Aeronautics and Astronautics,Washington, DC, 1997), AIAA 97-3052.
[11] S. Barral, K. Makowski, Z. Peradzynski, N. Gascon, and M. Dudeck, Phys. Plasmas **10**, 4137 (2003).
[12] J. Vaughan, IEEE Trans. Electron Devices **36**, 1963 (1989).
[13] C. Ordonez and R. Peterkin, J. Appl. Phys. **79**, 2270 (1996).
[14] E. Ahedo, Phys. Plasmas **9**, 3178 (2002).
[15] V. Smirnov, Sov. J. Plasma Phys. **5**, 202 (1979).
[16] M. Keidar, I. Boyd, and I. Beilis, Phys. Plasmas **8**, 5315 (2001).
[17] L. Tonks and I. Langmuir, Phys. Rev. **34**, 876 (1929).
[18] R. Goldston and P. Rutherford, *Introduction to Plasma Physics* (Institute of Physics, Bristol, 1995), p. 172.